



HAL
open science

Exolysin (ExlA) from *Pseudomonas aeruginosa* Punctures Holes into Target Membranes Using a Molten Globule Domain

Quentin Bertrand, Viviana Job, Antoine Maillard, Lionel Imbert, Jean-Marie Teulon, Adrien Favier, Jean-Luc Pellequer, Philippe Huber, Ina Attree, Andréa Dessen

► To cite this version:

Quentin Bertrand, Viviana Job, Antoine Maillard, Lionel Imbert, Jean-Marie Teulon, et al.. Exolysin (ExlA) from *Pseudomonas aeruginosa* Punctures Holes into Target Membranes Using a Molten Globule Domain. *Journal of Molecular Biology*, 2020, 432 (16), pp.4466-4480. 10.1016/j.jmb.2020.05.025 . hal-02909708

HAL Id: hal-02909708

<https://hal.univ-grenoble-alpes.fr/hal-02909708>

Submitted on 13 Jan 2021

HAL is a multi-disciplinary open access archive for the deposit and dissemination of scientific research documents, whether they are published or not. The documents may come from teaching and research institutions in France or abroad, or from public or private research centers.

L'archive ouverte pluridisciplinaire **HAL**, est destinée au dépôt et à la diffusion de documents scientifiques de niveau recherche, publiés ou non, émanant des établissements d'enseignement et de recherche français ou étrangers, des laboratoires publics ou privés.



Exolysin (ExlA) from *Pseudomonas aeruginosa* Punctures Holes into Target Membranes Using a Molten Globule Domain

Quentin Bertrand¹, Viviana Job², Antoine P. Maillard², Lionel Imbert¹, Jean-Marie Teulon¹, Adrien Favier¹, Jean-Luc Pellequer¹, Philippe Huber², Ina Attrée² and Andréa Dessen^{1,3}

1 - Univ Grenoble Alpes, CNRS, CEA, Institut de Biologie Structurale (IBS), F-38044 Grenoble, France

2 - Univ Grenoble Alpes, CNRS ERL5261, CEA-IRIG-BCI, INSERM UMR1036, Grenoble 38000, France

3 - Brazilian Biosciences National Laboratory (LNBio), CNPEM, Campinas 13084-971, São Paulo, Brazil

Correspondence to Andréa Dessen: Institut de Biologie Structurale, Bacterial Pathogenesis Group, Grenoble, France. andrea.dessen@ibs.fr

<https://doi.org/10.1016/j.jmb.2020.05.025>

Edited by C. Kalodimos

Abstract

Bacteria employ several mechanisms, and most notably secretion systems, to translocate effectors from the cytoplasm to the extracellular environment or the cell surface. *Pseudomonas aeruginosa* widely employs secretion machineries such as the Type III Secretion System to support virulence and cytotoxicity. However, recently identified *P. aeruginosa* strains that do not express the Type III Secretion System have been shown to express ExlA, an exolysin translocated through a two-partner secretion system, and are the causative agents of severe lung hemorrhage. Sequence predictions of ExlA indicate filamentous hemagglutinin (FHA-2) domains as the prevalent features, followed by a C-terminal domain with no known homologs. In this work, we have addressed the mechanism employed by ExlA to target membrane bilayers by using NMR, small-angle X-ray scattering, atomic force microscopy, and cellular infection techniques. We show that the C-terminal domain of ExlA displays a “molten globule-like” fold that punctures small holes into membranes composed of negatively charged lipids, while other domains could play a lesser role in target recognition. In addition, epithelial cells infected with *P. aeruginosa* strains expressing different ExlA variants allow localization of the toxin to lipid rafts. ExlA homologs have been identified in numerous bacterial strains, indicating that lipid bilayer destruction is an effective strategy employed by bacteria to establish interactions with multiple hosts.

© 2020 Elsevier Ltd. All rights reserved.

Introduction

Microbial pathogens have developed multiple means to subvert target cell functions in order to facilitate infection or outgrow competing bacteria in polymicrobial environments. Gram-negative bacteria possess a number of translocation nanomachines that deliver proteins, small molecules, or DNA across the cell envelope to the external surroundings or directly into the cytoplasm of target cells. One of the most well-studied of these machineries, the Type III Secretion System (T3SS), translocates toxins directly from the bacterial cytoplasm into that of its eukaryotic target, bypassing periplasmic, outer membrane, and extracellular steps. The T3SS

represents one of the most widespread molecular weapons involved in bacterial pathogenesis and colonization, being essential for the establishment of these processes by Gram-negative bacteria [1,2].

Pseudomonas aeruginosa is a major human nosocomial pathogen that makes use of different secretion systems, including the T3SS, to establish infection. Recently, however, *P. aeruginosa* strains lacking T3SS genes were isolated from different types of infection sites, including from patients suffering from an aggressive form of hemorrhagic pneumonia [3,4]. The hyper-virulence of these T3SS-free *P. aeruginosa* strains is determined by the presence of Exolysin A (ExlA), a toxin that displays cell membrane perforating activity and

provides a cytolytic phenotype on non-cytotoxic strains [3,5]. ExIA-dependent pore formation allows both Ca^{2+} influx and K^+ efflux, thus hijacking cell signaling pathways that control epithelial integrity [6] or macrophage cell death [7]. ExIA-positive *P. aeruginosa* strains have now been found worldwide in patients with various types of infection and are widespread in the environment [4]. ExIA belongs to the family of hemolysins and hemagglutinins, molecules exported by two-partner secretion (TPS) systems (a subtype of the Type V Secretion System, or T5SS). The family also includes the FHA filamentous hemagglutinin from *Bordetella pertussis* [8] and the ShIA hemolysin from *Serratia marcescens* [9], with which ExIA shares 32 % sequence identity.

Typical TPS systems are composed of a passenger protein (TpsA) and its cognate transporter (TpsB), both of which are encoded on the same operon. TpsAs are very diverse in size and function, but they all display a conserved, 300-residue long TPS domain at their N terminus, downstream from the secretion signal. TpsBs, on the other hand, are 60-kDa outer-membrane proteins from the Omp85 transporter superfamily, where a 16-stranded β -barrel is preceded by periplasmic polypeptide transport-associated (POTRA) domains [10]. In the case of ExIA, the toxin is encoded within a two-gene operon (*exIB-exIA*) where *exIB* corresponds to the TpsB. ExIB is also predicted to carry POTRA domains, whose function would be to recognize the TPS domain of ExIA in an in an unfolded conformation, and aid in its threading through the β -barrel, thus allowing translocation and secretion to the outside of the bacterium [11,12].

Notably, the TPS system mainly secretes virulence factors that target eukaryotic cells, but is also important for biofilm formation and cellular adherence [13–15]. In addition, the TPS system can also target other bacteria through a contact-dependent growth inhibition (CDI) mechanism where a stalled, partially secreted state ensures that TpsA is only secreted upon contact with the target bacterium, as is the case for the recently reported CdiA toxin from *Escherichia coli* [16]. CdiA harbors both FHA-1 and FHA-2 domains, with a toxin domain being present at the C terminus of FHA-2. FHA-1 repeats were initially identified in the filamentous hemagglutinin adhesin from *Bordetella* spp. [17] and subsequently shown to fold into an elongated β -helix [18–20]. In the case of CdiA, only the FHA-1 sequences fold into filaments that extend from the bacterial surface, while FHA-2, and the toxin region, remain within the originating bacterium until a target receptor is recognized. Upon recognition, a conformational change ensures that both FHA-2 domains become inserted in the outer membrane of the target cell and act as a translocon, delivering the toxin domain to the periplasm [16].

In the case of ExIA, FHA-2 repeats are predicted to be present throughout much of the polypeptide, with the exception of its C-terminal domain (Figure 1(a)). Notably, despite the fact that the extreme C-terminal region of ExIA has been shown to carry pore-forming activity, the specificity, fold, and mechanism of action of ExIA remain unclear. In this work, small-angle X-ray scattering (SAXS), NMR, and bilayer recognition strategies were used to show that ExIA employs its C-terminal domain (ExIA_{Cter}), which folds as a molten globule, to recognize negatively charged lipids. In addition, atomic force microscopy (AFM) studies indicate that upon lipid recognition, ExIA_{Cter} forms small holes in lipid bilayers in a time- and concentration-dependent manner. Upon infection of epithelial cells, ExIA localizes to lipid rafts in a cholesterol-dependent manner. A form that does not carry the C-terminal domain can also bind to lipid rafts and induce membrane destabilization, albeit with slower kinetics than the full-length form.

Results

Structural characterization of ExIA_{Cter}

The C-terminal regions of proteins of the filamentous hemagglutinin family have been shown to play different roles upon interacting with their targets, and this is also the case for ExIA. The C-terminal region of ExIA shares no homology with any other protein of known function, and this region was shown to be important for the cytotoxicity of ExIA toward epithelial cells. In addition, the purified form of the domain was shown to disrupt phospholipid bilayers in a liposome leakage assay, albeit uniquely at pH 4.0 [5]. These observations suggested that low pH could induce a change that mimics a conformation relevant for membrane targeting in a cellular environment.

In order to gain insight into the fold of ExIA_{Cter} in solution, we performed SAXS measurements with the protein at pH 4.0 and 7.5. Scattering patterns were recorded at different concentrations and the data were plotted in the form of $I(s)$ versus q (nm^{-1}) with PRIMUS [21]. The Guinier plots were linear, and data at low angles did not indicate any significant aggregation. Figure 1(b) shows the merged scattered data, which were used to generate the pair distribution plots $p(r)$ using GNOM [22], that provided information on the positions of electrons within the scattering samples. The real space gyration radius (R_g) and the D_{max} were determined from the $p(r)$ curves of ExIA_{Cter} (Figure 1(b)) [23] and correspond to 4.86 and 15.42 nm, respectively, indicating that the molecule could be elongated. In addition, the overall shape of the Kratky plot indicates that ExIA_{Cter} is flexible at both pH values tested. These observations were supported by a disorder prediction analysis performed with

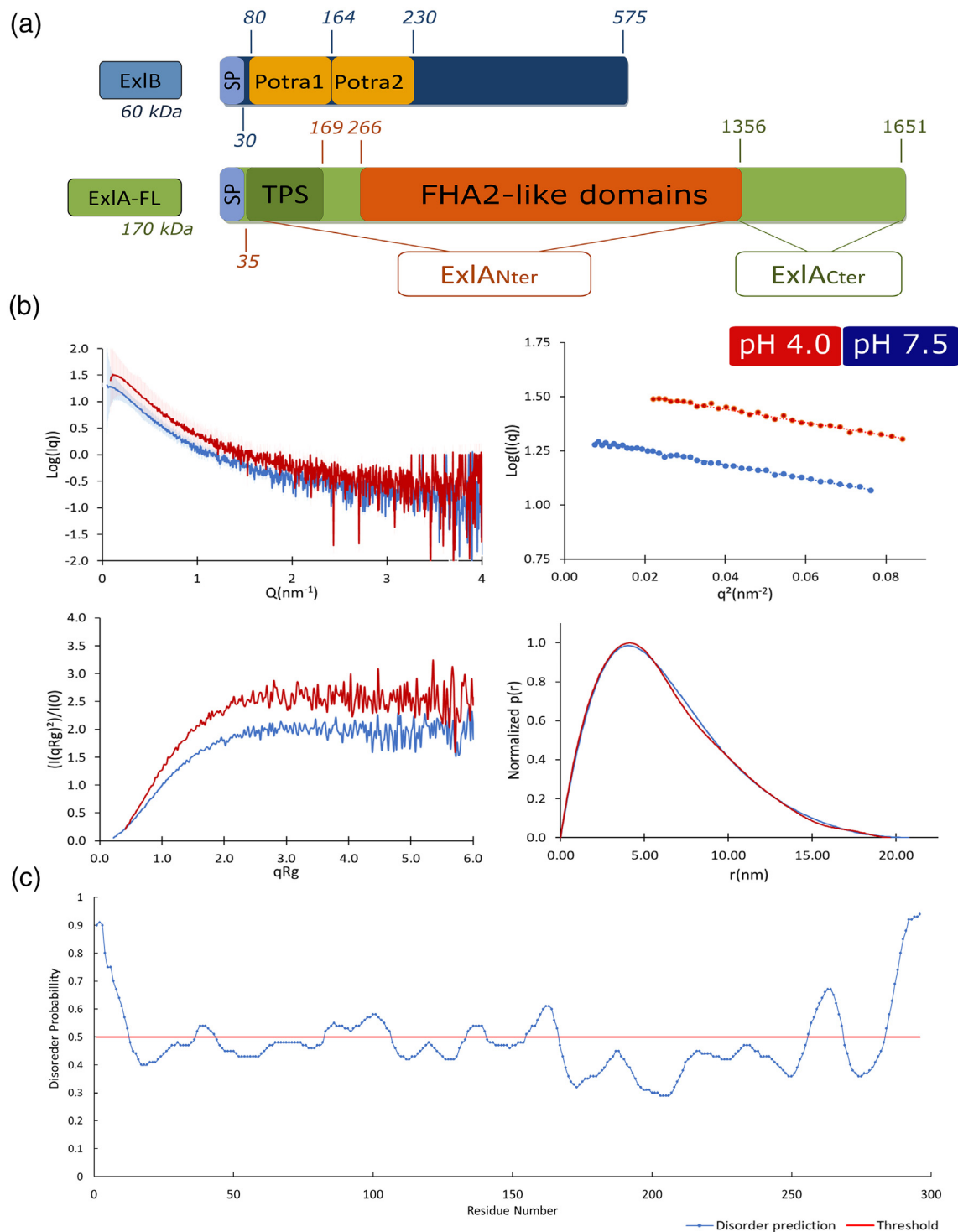


Figure 1. ExIA is a multi-domain, flexible protein. (a) Schematic diagram of predicted domain delimitations in both ExIB and ExIA. ExIA constructs used in this work are also indicated. SP, signal peptide. TPS, two-partner secretion. Residue numbers delimiting the different domains are shown. (b) SAXS analysis of ExIA_{Cter} at pH 4.0 (in red) and pH 7.5 (in blue). Upper left, raw scattering curves. The radially averaged scattered X-ray intensity (I) was plotted as a function of the scattering angle (q). Upper right, Guinier plot. The bottom left panel shows the Kratky plot, with the overall shape of the curve indicating that the molecules are flexible. The right bottom panel shows a plot of pair-distance distribution function; $p(r)$ for the two samples. The characteristic bell shape with an elongated shoulder indicates that the molecules are elongated. (c) PrDOS plot of ExIA_{Cter} indicating that the threshold of 0.5 for disorder probability is surpassed multiple times throughout the entire sequence.

PrDos [24], which indicates that disorder can be identified throughout the entire sequence, with the exception of a more stable region between residues 180 and 250 (Figure 1(c)).

SAXS experiments were complemented with an 1D ^1H NMR approach in order to obtain an idea of the structural compactness of the sample [25]. Spectra of ExIA_{Cter} were measured at both pH 4.0 and pH 7.5. Figure 2 shows that only a few peaks are visible in the folded NH region from 10 to 8.5 ppm at both pH values, indicating that ExIA_{Cter} is partially unfolded. Furthermore, the HET-SOFAST experiments generated λ_{NOE} values of 0.5 for the experiment performed at pH 4.0 and 0.7 for the one at pH 7.5. The λ_{NOE} is directly related to the compactness of a given molecule in solution and

can range from 0.35 for a compact protein to 0.75 for a disordered sample [25]. This indicates that ExIA_{Cter} at pH 7.5 mostly resembles an unfolded polypeptide chain, while at pH 4.0, increased compactness is suggestive of a molten globule-like state.

The C terminus of ExIA binds to and punctures holes in negatively charged lipid bilayers

Since ExIA forms pores in host membranes [3,5], we hypothesized that the molten globule conformation of its C-terminal domain could be a transient state that could recognize specific lipids. In order to test this possibility, we performed protein–lipid overlay assays using “lipid strips” that were incubated with purified ExIA_{Cter} and developed with anti-

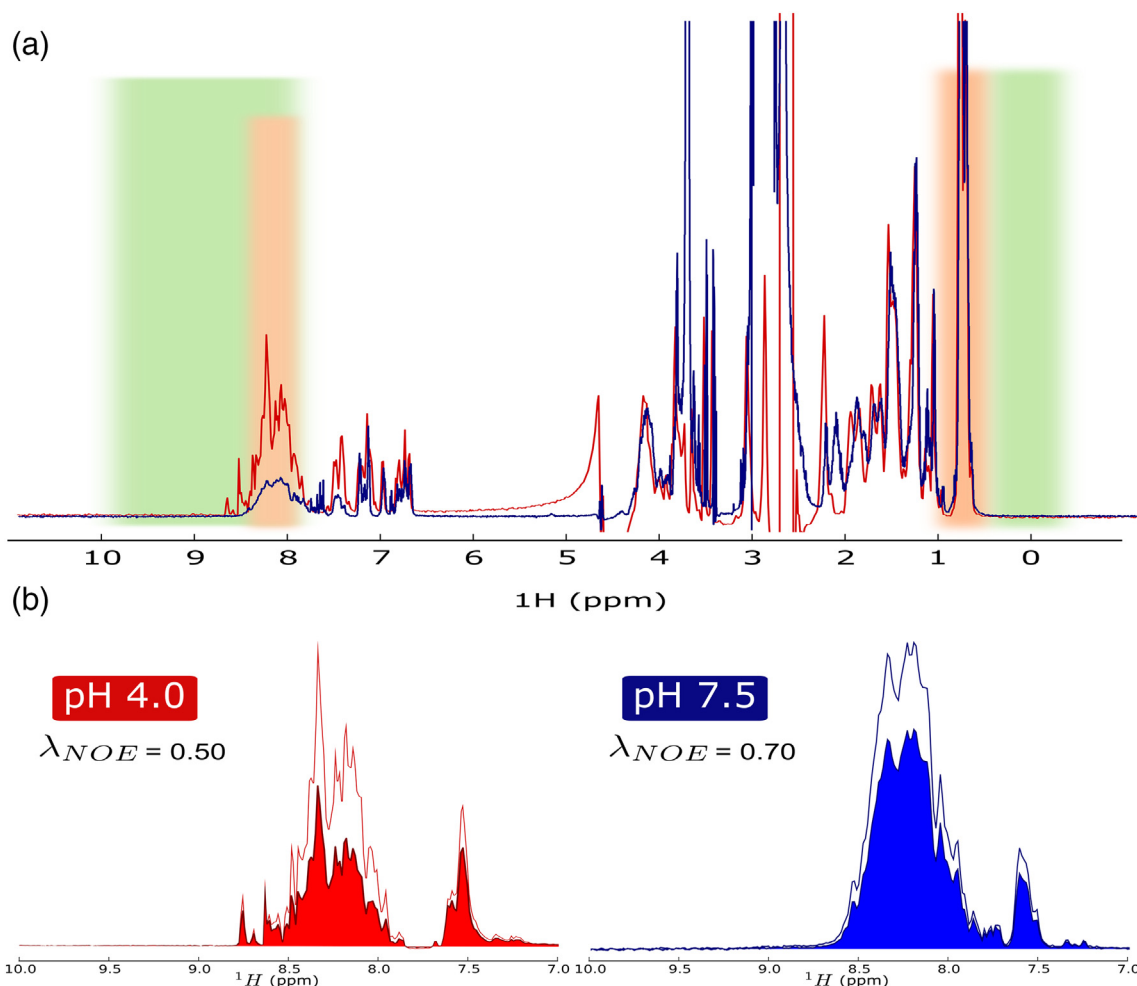


Figure 2. The C-terminal domain of ExIA displays a molten globule-like state. (a) Superposition of the two 1D ^1H NMR spectra recorded for ExIA_{Cter}. The red curve represents data recorded at pH 4.0, and the blue one at pH 7.5. The shaded boxes highlight the regions in the spectrum where peaks would be expected when the sample is folded (green) or unfolded (orange). (b) Overlay of 1D ^1H spectra of HET-SOFAST experiments allowing for the quantification of the structural compactness of ExIA_{Cter}. The λ_{NOE} value corresponds to the ratio of the integral of the saturated spectrum highlighted with the filled color divided by the integral of the reference spectrum shown with a thin line. A fully folded protein generates λ_{NOE} values in the range of 0.3 to 0.4, while unfolded molecules generate values above 0.7 [25].

ExIA antibodies. ExIA_{Cter} was shown to interact with phosphatidic acid (PA), phosphatidylinositols (PI_xP), phosphatidylserine (PS), and cardiolipin (CL) (Figure 3(a)). These negatively charged lipids participate in eukaryotic cell signaling processes, with PI_xP, PA and PS being preferentially (but not exclusively) located within the cytoplasmic side of eukaryotic membranes [26,27]. The ability of ExIA_{Cter} to preferentially bind to inner leaflet phospholipids suggests that, in a setting where the bacterium is in close contact with a eukaryotic cell, this region could be its final target, thus explaining the bilayer disruption effect.

In order to further explore details of membrane association of ExIA_{Cter}, we incubated the purified protein with artificial liposomes composed of 1-palmitoyl-2-oleoyl-sn-glycero-3-phospho-L-serine (POPS), phosphatidylcholine (PC), and cholesterol, and separated soluble from membrane-bound proteins on sucrose gradients. A full-length version of the molecule (ExIA-FL), as well as one lacking the C-terminal domain (ExIA_{Nter}), were also tested in order to clarify which ExIA domains are involved in bilayer recognition. Sucrose gradient samples were ultracentrifuged, and individual fractions were analyzed by SDS-PAGE (Figure 3(a)). Control liposomes, which were not incubated with the proteins, repeatedly migrated on fraction 2 of the gradients

and were visible as a thin white compact band. Interestingly, upon incubation with ExIA, we observed the appearance of a new white layer below the one corresponding to intact liposomes (fractions 4–6). Notably, both ExIA-FL and ExIA_{Cter} floated mostly in fractions 4–6, indicating that in addition to binding to liposomes, they seem to also disrupt their structure, causing them to float slightly lower in the gradient than the protein-free liposomes. On the other hand, ExIA_{Nter} did not demonstrate any significant binding to liposomes, migrating at the bottom of the gradient as in the experiment performed in the absence of lipids. These results thus indicate that it is the C-terminal domain of ExIA that plays the major role in bilayer recognition *in vitro*, in agreement with the observation that a *P. aeruginosa* strain expressing an ExIA variant that lacks this domain is unable to efficiently lyse epithelial cells [5].

Membrane binding by ExIA_{Cter} was further characterized by AFM. Liposomes composed of 4:1 PC:POPS supplemented with 10 % cholesterol were used to reconstruct supported lipid bilayers on a mica support. Membranes were then incubated with ExIA_{Cter}, and AFM images were acquired at different time points ranging from 5 to 30 min post-incubation. Control liposomes revealed mostly flat lipid bilayers (Figure 4(a)), but upon addition of ExIA_{Cter} at a concentration of 1 nM, small holes appeared on the

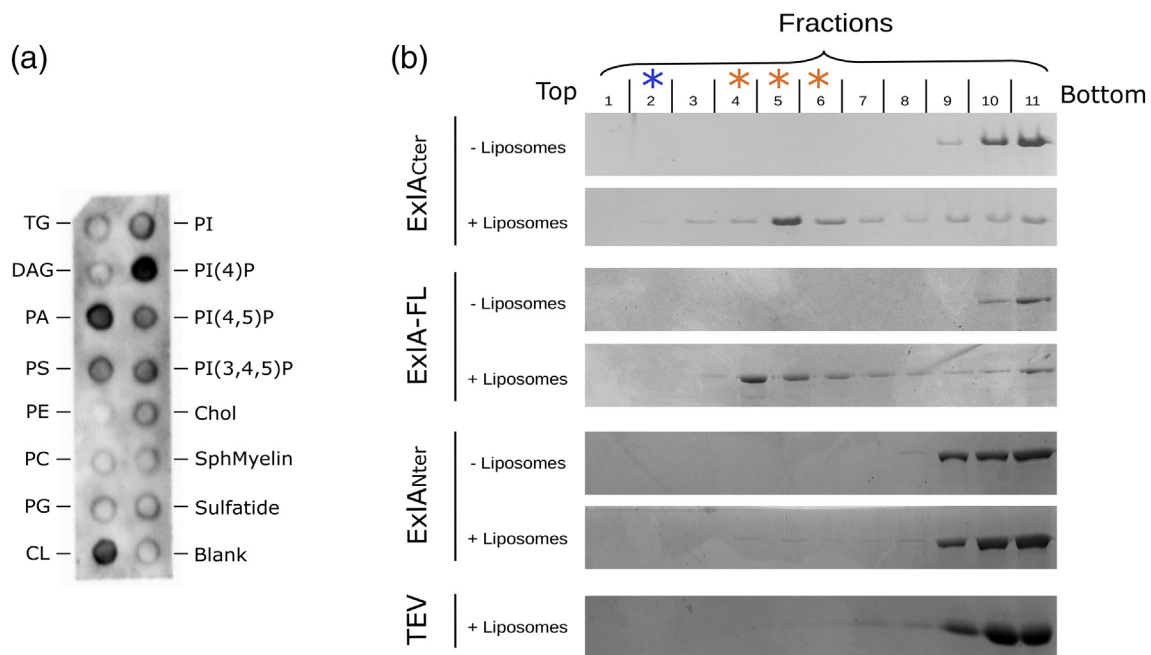


Figure 3. ExIA interacts with lipids. (a) Protein–lipid overlay test showing the interaction of ExIA_{Cter} with PA (phosphatidic acid), phosphatidylinositol (PI_xP), phosphatidylserine (PS), and cardiolipin (CL). (b) Insertion of ExIA into liposomes. Purified ExIA variants were incubated with liposomes containing 4:1 PC:POPS + 5 % cholesterol and separated by sucrose gradient ultracentrifugation. Intact liposomes migrated in fraction 2 (blue star), while proteoliposomes migrated below (orange stars). SDS-PAGE of fractions indicate that only full-length ExIA (ExIA-FL) and ExIA_{Cter} were able to bind liposomes efficiently and float in fractions 4–6. Tobacco etch virus (TEV) protease was used as a negative control.

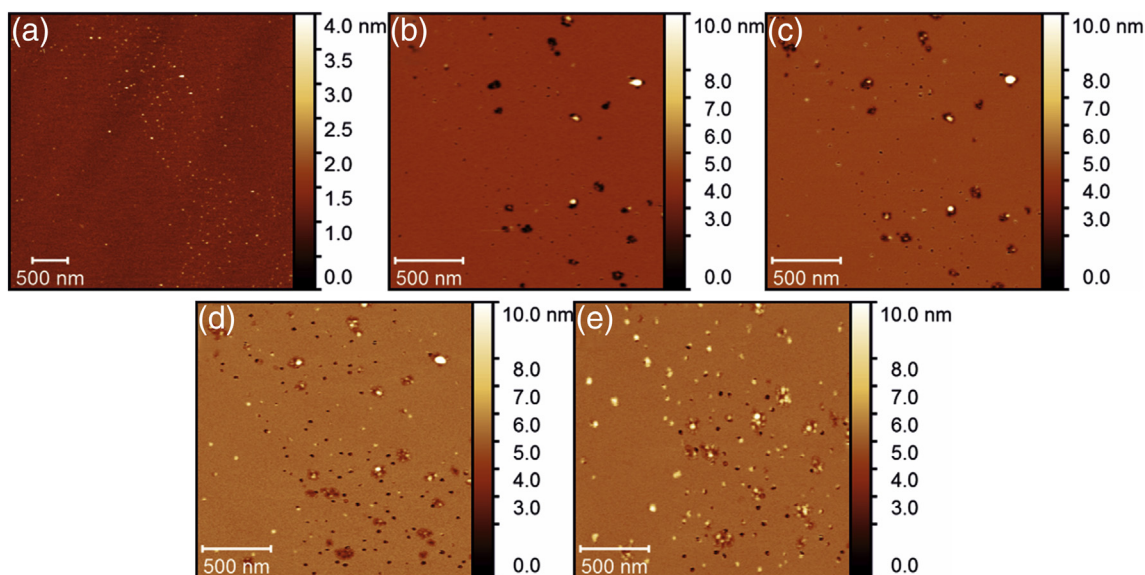


Figure 4. Time sequence imaging of ExIA_{Cter} by AFM on supported membrane bilayers in a buffered environment. (a) Control image of 4:1 PC:POPS + 10 % cholesterol supported bilayer. (b) Injection of 1 nM ExIA on the supported membrane bilayers (a) with the same scan size (4 μ m) but cropped at 2 μ m to match the images that follow. (c–e) Continuous imaging of supported membrane bilayers on a smaller scan size to emphasize the sizes of holes in membranes (2 μ m). It can be seen that upon introduction of ExIA_{Cter}, the roughness of the membrane increases, the average surface area of holes decreases, and the depth of holes increases from 1.5 nm in (b) to 3.4 nm in (e). At a scan rate of 1 Hz, the time between each image (b–e) is about 8.5 min; thus, the end of image (e) was at 34 min post-ExIA injection.

membrane in the form of dark spots. Interestingly, over time, both the number of holes and membrane roughness increased and were accompanied by the appearance of white spots, possibly aggregated lipids and/or protein (compare Figure 4(b) and (d)). However, after approximately 30 min of incubation, the number of holes as well as their size decreased (Figure 4(e)), which was concomitantly linked with an increase in hole depth (Table 1). These observations indicate that the C-terminal domain of ExIA affects the integrity of artificial bilayers by puncturing the membrane, even in the absence of other regions of the toxin and/or other receptors or partner proteins. Since the ability of ExIA_{Cter} to puncture bilayers could also be directly related to the extreme cytotoxicity of the full-length molecule, we set out to study the effect of different forms of ExIA in a cellular setting.

Table 1. Time-lapse geometric characterization of holes observed on supported lipid bilayers.

Image	Roughness Sq (nm)	Nb open holes	Average depth of open holes (nm)	Surface area of open holes (nm ²)
A	0.162	1	0.10	300
B	0.244	65	1.54	1090
C	0.289	102	1.62	765
D	0.345	156	2.58	425
E	0.360	36	3.40	325

Full-length ExIA localizes to lipid rafts

P. aeruginosa strains expressing ExIA induce death of eukaryotic cells by formation of pores in membranes [5], but details of membrane recognition mechanisms are still unclear. In order to obtain further insight into this process, we infected eukaryotic epithelial A549 cells with the ExIA-positive *P. aeruginosa* strain IHMA879472 [4]. Infected cells were harvested and treated with the non-ionic detergent Triton X-100 to dissolve detergent-soluble membranes (DSM). Detergent-resistant membranes (DRM) containing lipid rafts were then isolated by sucrose gradient ultracentrifugation and fractions were analyzed by Western blotting. As shown in Figure 5, ExIA co-migrated with lipid rafts (fractions 2–3), as identified by the presence of flotillin-2, a protein marker of DRM, and was not present in the non-lipid raft fractions (fractions 9–12). Rho, a cytosolic protein, was identified in the latter fractions. Strikingly, when eukaryotic epithelial cells were infected by bacteria expressing ExIA_{Nter}, this form of the protein (that lacks the molten globule-like C-terminal domain) was also found in lipid raft fractions. This indicated that other domains of ExIA could also have lipid-recognition properties in cellular settings (Figure 5(b)). Subsequently, we examined whether ExIA detected in fractions 2–3 could come from residual bacteria still present in the eukaryotic

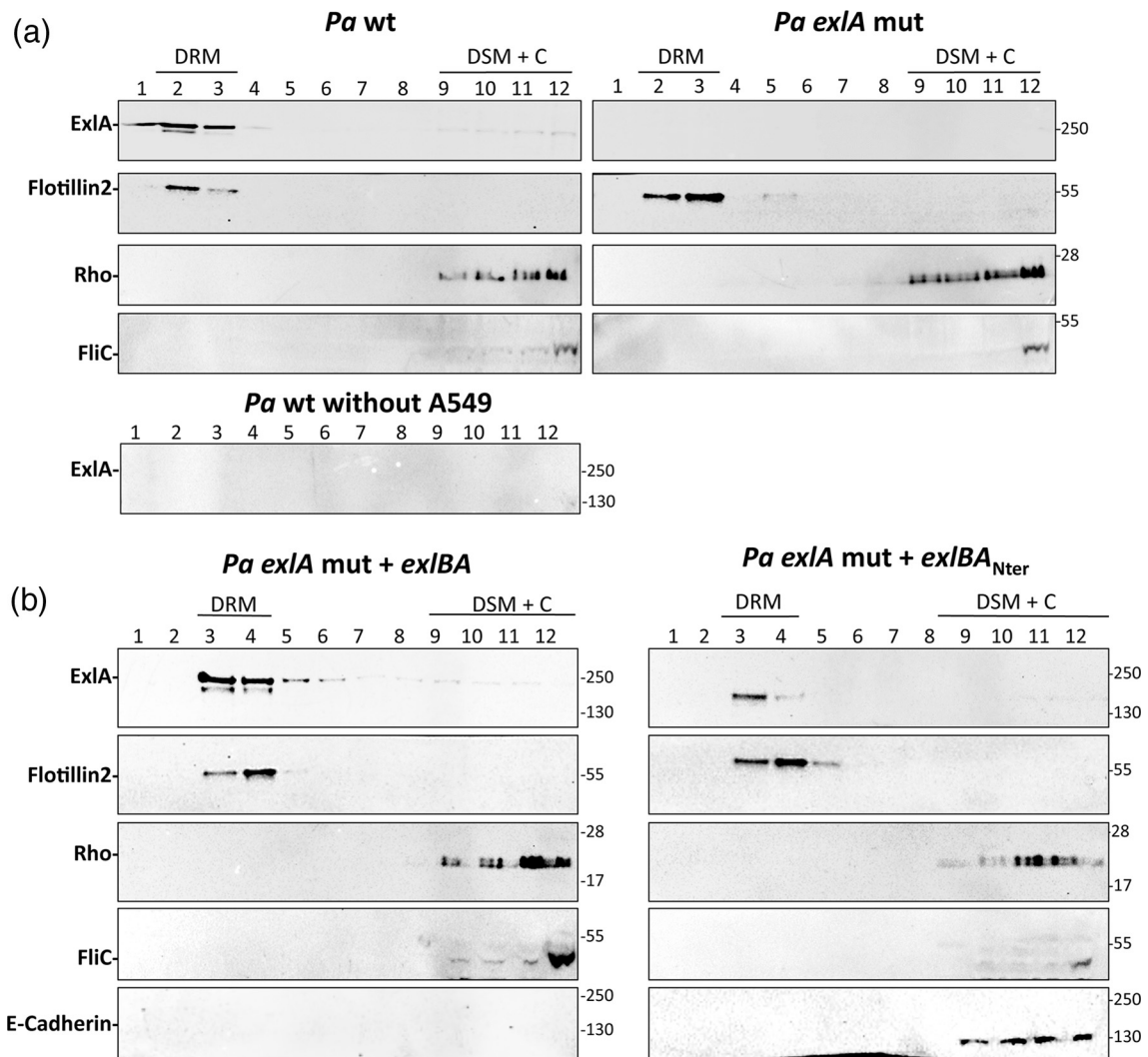


Figure 5. ExIA is inserted into lipid rafts. A549 cells were infected with *P. aeruginosa* strains as indicated, as described in [Materials and Methods](#). After infection, cell membranes were treated with 1 % Triton X-100 to dissolve detergent-sensitive membranes (DSM), and the detergent-resistant membranes (DRM) were separated by sucrose gradient flotation. Fractions were analyzed by Western blotting after ultracentrifugation with anti-ExIA antibodies. Anti-Flotillin2 was used as a marker for lipid rafts, anti-Rho as a marker for cytoplasm content (C) and anti-FliC for bacterial presence. Anti-E-cadherin-FL was used as a control for calcium influx. Results from a negative control where only bacteria (without A549 cells) were employed are shown at the bottom of (a). Note the association of both ExIA and ExIA_{Nter} with DRM (in (b)).

cell sample by performing a similar experiment that included bacteria but not A549 cells ([Figure 5\(a\)](#), bottom panel). Under these conditions, ExIA was not detected in any of the fractions, indicating that ExIA identified in fractions 2–3 in the previous experiment was indeed embedded in host cell membranes. Notably, FliC, a major component of the bacterial flagellum, was detected only in fraction 12 in all experiments; this corresponds to debris from bacteria present in the lysates.

Lipid rafts are known to be enriched in proteins/receptors involved in cell signaling and to contain high concentrations of cholesterol and sphingolipids [28]. In order to further investigate ExIA's localization

profile, we investigated the requirement of cholesterol for toxin association with rafts. We thus pre-treated eukaryotic epithelial A549 cells with methyl- β -cyclodextrin (M β CD), which extracts cholesterol from plasma membranes by destabilizing lipid rafts [29], and monitored ExIA incorporation into DRM after infection by performing sucrose gradient flotation and Western blotting experiments, as described above. As can be seen in [Figure 6](#), the treatment of cells with M β CD abolished almost all of ExIA's association with lipid rafts, and the toxin was present at the bottom of the gradient together with fractions containing soluble proteins. The presence of flotillin-2 in fractions 2–3 indicates that lipid rafts were not totally disrupted by

M β CD treatment, albeit sufficiently disrupted to delocalize ExIA from the rafts.

To examine whether M β CD-induced delocalization had an impact on ExIA toxicity, we incubated M β CD-treated A549 cells with the IHMA strain and measured propidium iodide (PI) incorporation into host cells, which reflects ExIA-dependent necrosis [6]. The results show that the M β CD treatment did not affect ExIA activity, as both non-treated and M β CD-treated cells displayed the same kinetics of cytotoxicity (Figure 6(b)). Thus, ExIA incorporation into lipid rafts is not required for triggering cytotoxicity.

The N-terminal domain of ExIA also presents cytolytic properties

Since ExIA_{Nter} was shown to partition into lipid rafts (Figure 6) and destabilize red blood cell membranes

[5], we reexamined the contribution of this region of the molecule for cytotoxicity (Figure 7). The kinetics of PI incorporation into epithelial A549 cells infected with bacteria expressing either ExIA-FL or ExIA_{Nter}, both under control of an arabinose-inducible promoter, was evaluated. Cytotoxicity was measured in presence or absence of 0.05 % arabinose. As shown in Figure 7(b), both strains secreted comparable amounts of wild-type or ExIA_{Nter}, in either condition (presence or absence of arabinose), and both were able to induce cell death and PI incorporation. Surprisingly, bacteria expressing ExIA_{Nter} were still cytotoxic, in both uninduced and induced conditions, albeit with delayed kinetics when compared to the strain expressing ExIA-FL (Figure 7(a)). To further investigate whether the strain expressing ExIA_{Nter} could induce a similar type of toxicity as the strain expressing ExIA-FL, we monitored the cleavage of

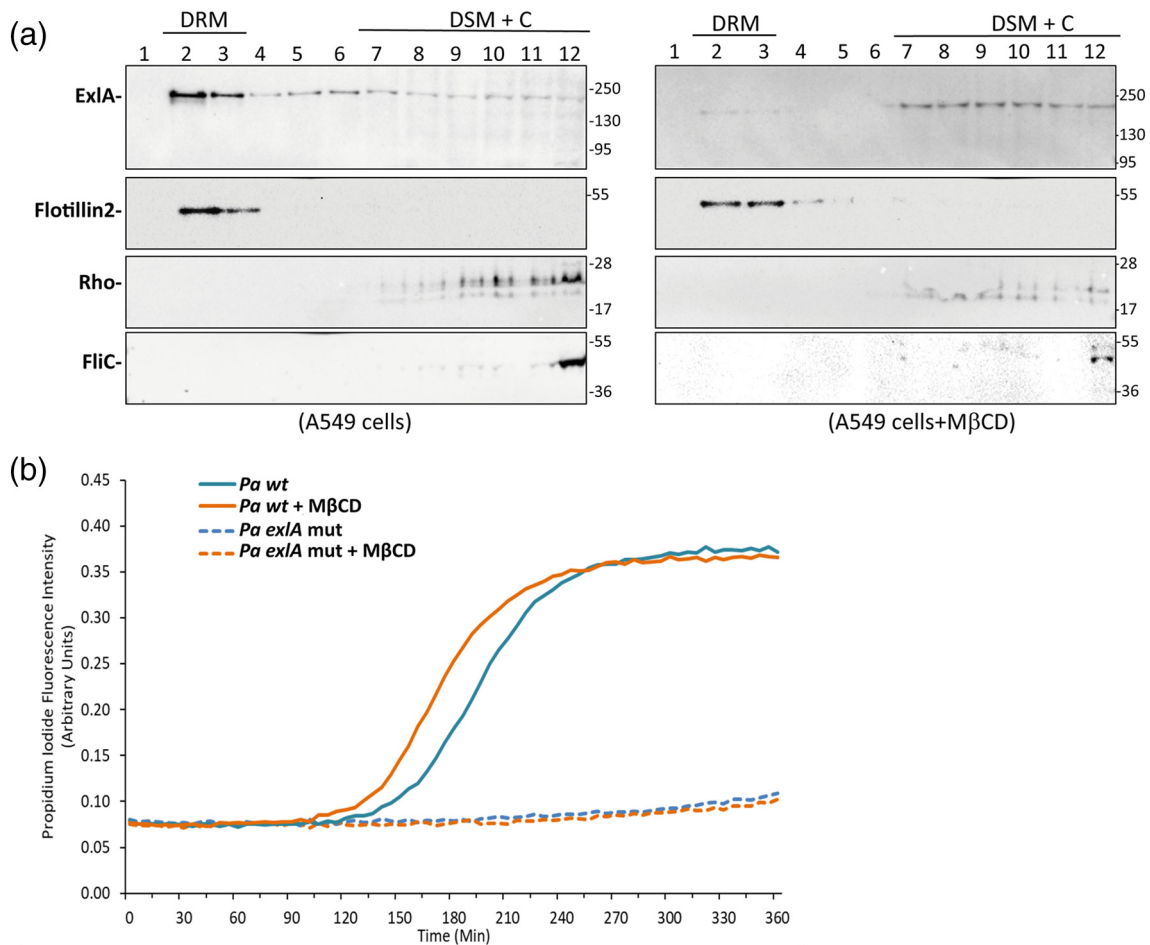


Figure 6. ExIA is removed from DRM after cholesterol depletion by M β CD treatment. (a) A549 epithelial cells were pretreated (right panel) or not (left panel) with m β CD in order to extract cholesterol from lipid rafts. Infection experiments were performed with *Pa wt* and *Pa exIA mut* for 2 h 30 min before cell washing, 1 % Triton X-100 incubation and the sucrose gradient ultracentrifugation. Fractions were loaded onto SDS-PAGE and analyzed by Western blotting as done for the experiment whose results are shown in Figure 5. DRM, detergent-resistant membranes; DSM, detergent-sensitive membranes; C, cytoplasm. (b) Propidium iodide incorporation during infection of A549 pretreated (orange) or not (blue) with m β CD.

E-cadherin, which is known to be induced by ExlA via a Ca^{2+} influx–calmodulin–ADAM10 pathway [6]. As shown in Figure 7(c), the overexpression of ExlA_{Nter} induced partial cleavage of E-cadherin, which was evidenced by the detection of its C-terminal fragment and the lower amount of full-length protein. Under the same conditions, the full-length form of ExlA triggered a complete cleavage of E-cadherin. Thus, our data indicate that in addition to the fact that the C terminus of ExlA is important for its pore-forming activity, the remainder of the protein carrying notably the FHA-2 domains also has the potential to bind to lipid rafts and induce membrane destabilization and E-cadherin cleavage, albeit with slower kinetics as compared to the full-length protein.

Discussion

Molecules translocated by bacterial secretion systems play key functions in infection and commensalism, including manipulation of target signaling pathways, overcoming of host immune systems, or providing advantages within polymicrobial environments. The well-studied T5SS requires the insertion of a β -barrel protein or domain (TpsB) in the outer bacterial membrane prior to threading of the activity-carrying molecule (TpsA) through the barrel. Most T5SS effector molecules are elongated, β -helical proteins, and both ExlA and ShlA from *S. marcescens* are also predicted to carry β -strand rich features in their N-terminal regions [6]. Notably, ShlA was shown to exert its pore-forming activity in a fashion that is distinct from that of the well-studied *E. coli* RTX toxins, the *Staphylococcus aureus* α -toxin or streptolysin O from group A β -hemolytic streptococci, and its action is dependent on the bacterial flagellar apparatus for target cell recognition [30–32]. In addition, the N-terminal region of ShlA is important for lipid binding [33]. These complex molecules, however, are challenging objects for biochemical studies due to the fact that they present both hydrophilic characteristics (in order to be soluble upon bacterial release) and hydrophobic (so as to bind to and exert their effects on target membranes) [33], are flexible, and tend to be prone to aggregation when their β -helical regions are not correctly capped [34]. This requires that such macromolecules be studied not only in their full-length forms, but also as individual domains. This strategy was employed in this work in the study of ExlA.

The combined data from 1D ^1H NMR and SEC-SAXS indicate that ExlA_{Cter} behaves as a molten globule in solution. Molten globule proteins exist in multiple transient states and can fold (fully or partially) upon binding to a partner [35]. Thus, it is conceivable that ExlA_{Cter} adopts a folded, more stable conformation when in contact with the target lipidic bilayer. This strategy would allow the bacterial cell to carry an aggressively cytotoxic molecule within its periplasm,

but which will only become active (and form pores) when it recognizes a negatively charged, eukaryotic membrane. This hypothesis is further supported by the fact that our bilayer studies show that ExlA binds mostly negatively charged lipids, such as PI₄P and PS, which are present on the cytoplasmic side of eukaryotic cell membranes.

Imaging of the action of ExlA_{Cter} on reconstituted supported lipid bilayers indicated that this domain, on its own, does not form organized oligomers around a central pore, as is the case for other well-studied pore-forming toxins [31], but rather forms holes of different dimensions, as evidenced by our AFM results (Figure 4). In our time-lapse experiment, the depth of holes continuously increased with time. This suggests that ExlA_{Cter}, rather than forming stable, fixed pores, acts by disrupting the membrane, causing the direct increase in roughness (Table 1). These experiments provided the first visual characterization of the direct effect of ExlA on target membranes.

Interestingly, the floating assay performed on eukaryotic cell membranes indicated that ExlA-FL localized to lipid rafts, i.e., cholesterol-rich regions of the membrane [28]. We employed M β CD to partially remove cholesterol from lipid rafts, reducing their integrity. The addition of M β CD did not impact ExlA cytotoxicity, indicating that cholesterol is not required for this activity. However, the depletion of cholesterol during infection caused the relocalization of ExlA from lipid rafts to the DSM regions, indicating that ExlA's interaction with the eukaryotic membrane could be mediated by lipids other than cholesterol or a potential partner whose localization could depend on the presence of cholesterol. Notably, the N-terminal region of ExlA plays an important role in this interaction, as is the case for ShlA [9], as mentioned above.

Lastly, from a more cellular viewpoint, monitoring of the survival of eukaryotic cells after infection with strains expressing ExlA-FL or ExlA_{Nter} indicated that despite the fact that the form of the toxin lacking the C terminus still displays some ability to infect cells, this is delayed when compared to strains expressing its full-length form. Thus, based on the data above and taking into account a model put forth for the well-studied filamentous hemagglutinin system [36,37], we can propose a model that describes functions for the different domains of ExlA. In the case of rapid kinetics, ExlA would first be targeted to membranes by the conformation imposed by ExlB during secretion, with its N-terminal domain being threaded first through the β -barrel pore. This would expose a molten globule region at the extremity of a potentially elongated structure containing β -helix features. The ExlA_{Cter} molten globule domain would recognize the negatively charged lipids on the target membrane. This intimate contact would trigger the formation of small pores, allowing Ca^{2+} influx [38] and engendering cell death. Notably, a slow kinetic model would involve other domains of ExlA in the membrane-binding step,

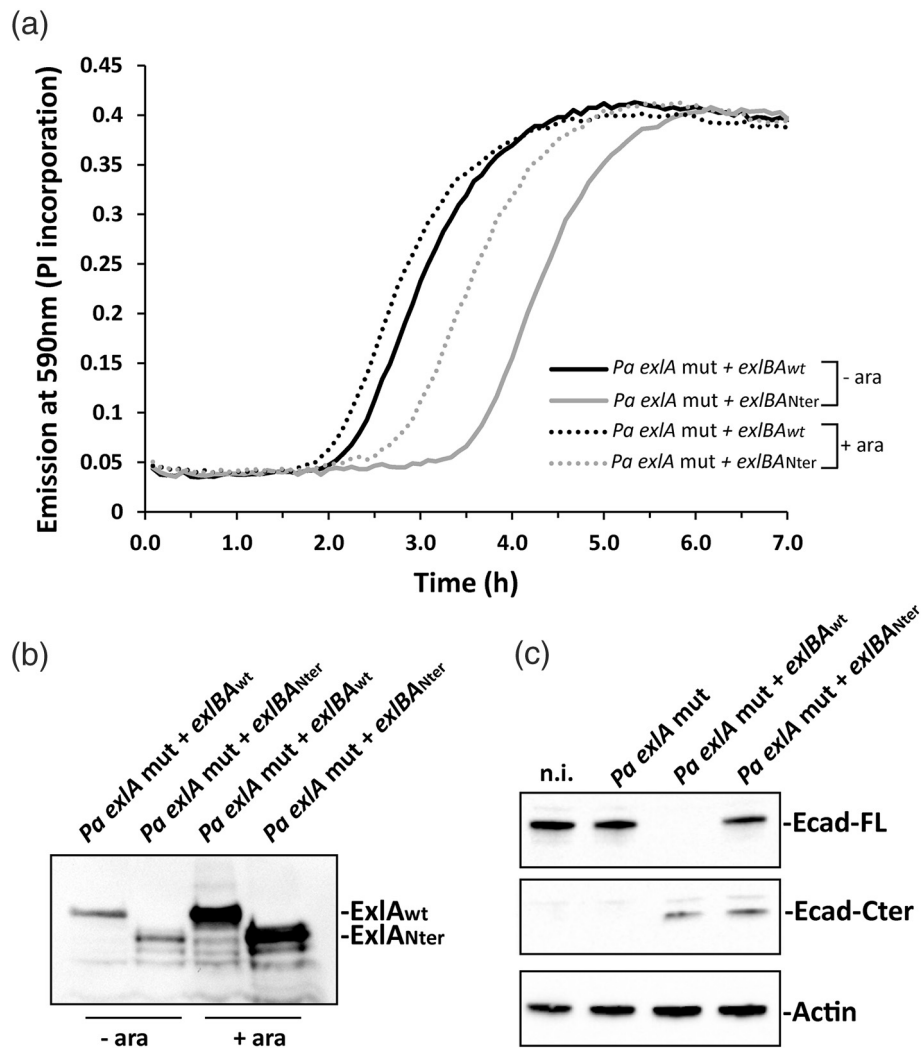


Figure 7. Cytotoxicity of ExIA_{Nter} (a) Toxicity of *Pa* strains (expressing ExIA_{Nter}) on A549 cells. Cells were infected at MOI 10 and necrosis was monitored by PI incorporation on a spectrofluorometer at different time points. (b) Analysis of ExIA quantities in secretomes of indicated strains revealed by Western blot. Bacteria were grown either in the absence or in the presence of 0.05 % arabinose (+ ara). (c) Western blot analysis of E-cadherin (E-cad) in A549 lysates infected by indicated strains. The non-infected control (n.i.) is also shown. Full-length (FL) E-cadherin (E-cad-FL) is shown above the cleaved C-terminal E-cadherin (E-cad-Cter) fragment, the latter indicating calcium influx. Actin was used as loading control.

such as the FHA-2 region. There is a precedent for the potential insertion of FHA-2 domains into membranes, as in the case of CdiA from *E. coli*, followed by translocation of a cytotoxic domain. However, in the case of CdiA, the interaction between the toxin and target cells is mediated by a receptor [16]. In the case of ExIA, despite the fact that it has not yet been shown, it cannot be excluded that certain eukaryotic cells may harbor a proteinaceous receptor that would regulate its recognition of the membrane. Genomic searches have identified ExIA-like molecules in diverse bacteria [11] and several environmental *Pseudomonas* spp. [39], indicating that eukaryotic membrane targeting is a mechanism of choice in the virulence factor arsenal of many bacteria that are capable of interacting with myriad hosts.

Materials and Methods

Cloning, cell-free expression, and purification

The sequence corresponding to ExIA_{Cter} was cloned into a pIVEX24 vector, which had its FactorXa-coding sequence removed, leaving only the region coding for a His₆ tag upstream from the ExIA_{Cter}-coding sequence (residues 1356 to 1651). Regarding the ExIA_{Nter} (residues 35 to 1356) and ExIA-FL (residues 35 to 1651) constructs, both genes were cloned without the ExIA signal peptide into a pET28 vector, leading to C-terminally His₆-tagged proteins.

ExIA_{Cter} was synthesized *in vitro* using a cell-free expression system (ISBG Grenoble). Briefly, ExIA_{Cter}

was expressed under RNase-free conditions in dialysis mode (typically 9 ml) for 16 h at 22 °C under gentle agitation. The cell-free reaction mixture contained 16 $\mu\text{g ml}^{-1}$ of ExIA_{Cter} DNA, 1 mM of each of the 20 essential amino acids, 0.8 mM rNTPs (guanosine-, uracil-, and cytidine-5'-triphosphate ribonucleotides), 1.2 mM adenosine-5'-triphosphate, 55 mM HEPES (pH 7.5), 68 μM folinic acid, 0.64 mM cyclic adenosine monophosphate, 3.4 mM dithiothreitol, 27.5 mM ammonium acetate, 2 mM spermidine, 80 mM creatine phosphate, 208 mM potassium glutamate, 16 mM magnesium acetate, 250 $\mu\text{g ml}^{-1}$ creatine kinase, 27 $\mu\text{g ml}^{-1}$ T7 RNA polymerase, 0.175 $\mu\text{g ml}^{-1}$ tRNA, and 400 $\mu\text{l ml}^{-1}$ S30 *E. coli* bacterial extract. After incubation, the entire reaction mix was diluted in Buffer A (50 mM HEPES (pH 7.5), 300 mM NaCl, and 25 mM imidazole) to a final volume of 45 ml and centrifuged for 45 min at 36,000g at 4 °C. The supernatant was applied onto a 5 ml Ni-NTA resin or His-Trap column that had been previously equilibrated in Buffer A at 4 °C. The column was washed with 8 % Buffer B (50 mM HEPES (pH 7.5), 300 mM NaCl, 500 mM imidazole) to eliminate residual contaminants, and the protein was eluted with 100 % Buffer B. Fractions containing ExIA_{Cter} were pooled and concentrated on a 10-kDa cutoff membrane and applied onto a Superdex 200 10/300 GL column previously equilibrated in 50 mM Tri-sodium citrate (pH 4.0), 300 mM NaCl or 25 mM HEPES (pH 7.5), 300 mM NaCl. Fractions containing ExIA_{Cter} were pooled and concentrated for further analysis.

ExIA_{Nter} was overexpressed in *E. coli* BL21(DE3). Cultures were grown in LB medium containing 30 $\mu\text{g/ml}$ kanamycin and were induced with 0.5 mM IPTG at the exponential phase and grown for 3 h at 37 °C. Cells were then centrifuged for 20 min at 4000 rpm, and the pellet was resuspended in 40 ml Buffer C (25 mM Tris-HCl (pH 8.0), 500 mM NaCl, and 10 mM Imidazole) supplemented with protease inhibitors (EDTA-free Complete tablet, ROCHE) and 1 mM PMSF. Cells were lysed by four passages in a microfluidizer cell disruptor at 15,000 psi. Cell debris were removed by ultracentrifugation at 108,000g for 30 min at 4 °C. The supernatant was applied onto a 5-ml His-Trap HP column (GE healthcare) equilibrated in buffer A. Contaminants were eliminated by a washing step with 5 % Buffer D (25 mM Tris-HCl (pH 8.0), 500 mM NaCl, 500 mM imidazole). The His₆-tagged ExIA_{Nter} was eluted in 30 % Buffer D. The fractions of interest were pooled and concentrated using a Vivaspin 30 concentrator and applied onto a Superdex 200 HR 10/30 Increase column (GE Healthcare) equilibrated in 25 mM Tris-HCl (pH 8.0), 250 mM NaCl, and 1 mM EDTA. It is of note that on gel filtration ExIA_{Nter} eluted in two peaks, one in the void volume (at $V = 7.5$ ml) and one at $V = 9$ ml that could correspond to a globular protein of 440 kDa (with a Stokes radius of 65.6 Å). Fraction purity was analyzed by SDS-PAGE and mass spectrometry.

ExIA-FL was expressed and purified as described above for ExIA_{Nter}, the only modification being that the culture was grown at 16 °C ON after IPTG induction. Following the His-Trap step, the sample was concentrated on a Millipore 100-kDa cut-off concentrator and subsequently injected onto a Superose 6 HR Increase column equilibrated in the gel filtration buffer described above. ExIA_{Nter} and ExIA-FL samples were then used for liposome interaction experiments.

Bacterial growth conditions and genetic constructions

P. aeruginosa was grown in LB medium at 37 °C with shaking. For all experiments, cultures were started at $\text{OD}_{600} = 0.1$ A.U. from an overnight culture. For epithelial cell infection, the following strains were used: the wild-type IHMA strain (*exIA*⁺), IHMA *exIA mut* and IHMA *exIA mut* complemented with either pSW196-*exIB-exIA_{wt}* or pSW196-*exIB-exIA_{Nter}* [5]. The plasmids were introduced by triparental mating. pSW196 is an integrative plasmid carrying an arabinose-inducible promoter for protein expression. It is of note that even in the absence of arabinose, a basal expression of the protein was observed.

NMR

NMR experiments were recorded using a Bruker 600-MHz and a 950-MHz NMR spectrometer at the ISBG platform (PSB Grenoble). 1D spectra were recorded at 25 °C, using a sample at a concentration of 0.1 μM in 50 mM Tri-sodium citrate (pH 4.0), 300 mM NaCl or in 25 mM HEPES (pH 7.5), 300 mM NaCl. The HET-SOFAST experiment and the λ_{NOE} value calculations were performed according to Schanda and co-workers [25].

Disorder prediction calculations

The sequence corresponding to ExIA_{Cter} (excluding the histidine tag) was submitted to the PrDOS [24] server to test for disorder propensity of the chain. A conservative value of 5 % for the rate of false positives was used as input for the disorder prediction threshold. Using these limits, residues presenting disorder probabilities above 0.5 are considered as being localized within disordered regions.

SEC-SAXS

SEC-SAXS data were recorded at the ESRF (Grenoble, France) on the BM-29 BIOSAXS beamline equipped with a Pilatus 1 M detector at a wavelength of 0.99 Å and at a 2.867-m sample-to-detector distance. Measurements were carried out using a 1-mm capillary cell, with a sample holder temperature kept constant at 20 °C. The size of the

beam at the sample was 700 μm * 700 μm and the s -range extended from 0.025 to 5 nm^{-1} .

Samples were applied onto a Superdex 200 10/300 GL column equilibrated in either 50 mM Tri-sodium citrate (pH 4.0), 300 mM NaCl or in 25 mM HEPES (pH 7.5), 300 mM NaCl. Data reduction included averaging of individual curves with PRIMUS from the ATSAS suite [40]. The radius of gyration, R_g , was

estimated using the Guinier approximation $I(s) = I(0)$

$\exp\left(-\frac{s^2 R_g^2}{3}\right)$, valid for small angles ($sR_g < 1.3$).

GNOM, from the ATSAS suite was used to obtain the distance distribution function, $p(r)$ as well as the maximum intramolecular distance.

Lipid strip tests

The ability of ExIA_{Cter} to recognize specific lipids was assessed using lipid strip overlay assays (Echelon). The tests were performed at room temperature, sheltered from light by aluminum foil, under mild agitation. Lipid strips were blocked with Tris-buffered saline supplemented with 0.03 % Tween-20 (TBS-T) and 3 % bovine serum albumin. ExIA_{Cter} was diluted to 80 nM in the same buffer and incubated with the lipid strip for 60 min. After the membrane was washed with TBS-T, it was probed with a mixture of polyclonal rabbit anti-ExIA antibodies diluted to 1/5000 [5]. Detection was performed by measuring chemiluminescence produced by horse radish peroxidase coupled to a goat anti-rabbit secondary antibody.

Liposome floating assay

Egg PC, POPS, and brain cholesterol were purchased from Avanti Polar Lipids. Liposomes were formed by mixing lipids at a mass ratio of 4:1 PC:POPS supplemented with 10 % cholesterol. Lipids were stored at -20 °C in chloroform; when needed, the required amounts were pipetted and mixed in a glass tube. A lipidic film was formed by chloroform evaporation under a nitrogen flux. Chloroform traces remaining in the sample were removed under a vacuum bell. The lipidic film was then suspended in a buffer matching the different ExIA purification buffers (50 mM Tri-sodium citrate (pH 4.0), 300 mM NaCl for ExIA_{Cter}; 50 mM HEPES (pH 7.5), 300 mM NaCl for ExIA_{Nter} and 50 mM HEPES (pH 7.5), 150 mM NaCl, 5 % glycerol and 8 M urea for ExIA-FL). For liposome floating assays, ExIA-FL was produced as previously described [5], except that the protein was obtained from solubilized inclusion bodies, using a method described by Burgess [41]. Liposomes were formed by extrusion of the previous solution through a mini-extruder (Avanti Polar Lipids) first with a 0.4- μm and subsequently with a 0.1- μm filter. Liposome homogeneity was assessed by Dynamic Light Scattering.

ExIA variants were incubated 2 h at room temperature with liposomes prepared in their respective buffers at a final concentration of 0.2 mg/ml of protein and 2.4 mg/ml of lipids. After incubation, 90 % sucrose was added to the sample to reach a final concentration of 45 %. Sucrose and buffer solutions were carefully pipetted onto the sucrose-sample mixtures to form a sucrose gradient ranging from 30 % to 10 %. Ultracentrifugation was performed in a SW55Ti rotor at 45,000 rpm for 17 h at 4 °C. Fractions at 500 μl were carefully pipetted from the tubes, and aliquots were separated on SDS-PAGE, which was stained with Coomassie blue.

Lipid raft purification

The epithelial lung carcinoma cell line A549 (ATCC CCL-185) was seeded in P100 dishes at 10^7 cells/dish and incubated at 37 °C with 5 % CO₂. Previous to infection fresh DMEM medium was added to each plate, with four plates being used per each condition. For cholesterol depletion experiments, A549 cells were incubated 2 h before infection in 1 mM M β CD. Bacterial cultures grown in LB media to OD₆₀₀ = 1.1 AU were added onto A459 monolayer cells with a multiplicity of infection of 10 at 37 °C under 5 % CO₂. The infection was followed by microscopy and was interrupted when about 70 % of cell shrinkage was visible (between 2.5 and 3 h). Subsequently, A549-infected cells were washed twice with 10 ml PBS and then resuspended into 0.4 ml/plates of 50 mM Buffer E (50 mM HEPES (pH 7.4), 150 mM NaCl, 5 mM EGTA, 1 % Triton X-100 containing a protease inhibitor cocktail (Complete, Roche)). The samples were incubated for 1 h on ice and kept in suspension by being vortexed frequently. Debris were subsequently eliminated by low speed centrifugation at 1000g for 10 min at 4 °C, and the supernatants were applied onto a sucrose gradient. Typically, 2 ml of 80 % sucrose in Buffer E were mixed with 2 ml of supernatant and loaded on the bottom of the centrifuge tube; 5 ml of 30 % sucrose and 3 ml of 5 % sucrose were then successively added on top. After ultracentrifugation in a SW41 Ti rotor at 40,000 rpm for 16 h at 4 °C, a cloudy white band became visible between the 5 % and 30 % sucrose layers, corresponding to lipid rafts. One-milliliter fractions were recovered from the top to the bottom of each tube, and samples were run on 4 %–12 % gradient SDS-PAGE Bis-Tris precast gels (BioRad), then transferred onto PVDF membranes for Western Blot analyses. Western blots were incubated with several antibodies: for ExIA, a mixture of rabbit polyclonal anti-ExIA antibodies against three ExIA-synthetic peptides [3] as well as anti-ExIA_{Cter} and anti-ExIA_{Nter} antibodies [42]; for E-cadherin, a mouse anti-E-cadherin C-ter antibody (Transduction Laboratories, clone 36); and for controls, mouse anti-Flotillin-2 (BD Biosciences, #610383), rabbit anti-Rho (ThermoFisher

Scientific PA5-101028), and rabbit anti-FliC antibodies [42].

Atomic force microscopy

Interactions between ExlA_{Cter} and reconstituted supported bilayers were imaged on a Multimode 8, NanoScope V (Bruker) equipped with NanoScope software (Bruker, Santa Barbara, CA) in fluid conditions. A 36- μ l drop of buffer (50 mM Tri-sodium citrate (pH 4.0), 300 mM NaCl) was deposited on a freshly cleaved mica, followed by a 4- μ l drop of liposome preparation. This mixture was left at room temperature for 2 h (45 °C) or overnight in a humid environment. Weakly bound material was removed by rinsing three times with 40 μ l of buffer (during each rinse, 40 μ l were removed and subsequently 40 μ l of fresh buffer were added). Before adding the protein, 40 μ l of buffer were deposited on the supported bilayers on the mica. Native membranes were imaged first and if a proper fusion was observed (large areas of uninterrupted supported bilayers), the drop was replaced by 40 μ l of fresh buffer. ExlA_{Cter} was then injected in the drop at the desired concentration. ScanAsyst fluid cantilevers ($k = 0.7$ N/m, $F_q = 150$ kHz, nominal tip radius = 20 nm, Bruker probes, Camarillo, CA, USA) were used. Images were collected at a rate of ~ 1 Hz, with 512 px on scan sizes varying from 4 to 2 μ m in length and using the ScanAsyst mode in a semi-automatic condition where both the gain and the setpoint were manually adjusted. The default ramp size for the peakforce mode was kept at 150 nm. Images were processed with Gwyddion [43], and if needed, stripe noise was removed using DeStripe [44]. Further image processing was performed using the Laplacian operator as described elsewhere [45].

Statistical analysis of AFM images was performed with Gwyddion. Holes in images were identified using the grain feature of Gwyddion using a low threshold value (between 3.5 and 4.5 nm) and by rejecting selections smaller than 5 pixels. The average depth of the holes was determined by measuring the median height of the membrane and subtracting the median height of holes. The surface area of holes was determined using the grain distribution function from Gwyddion and was converted into nm². Membrane roughness (Sq) was determined using Gwyddion's statistical quantities menu after removing holes in images.

CRedit authorship contribution statement

Quentin Bertrand: Methodology, Validation, Investigation, Writing - review & editing. **Viviana Job:** Methodology, Validation, Investigation, Writing - review & editing. **Antoine P. Maillard:** Methodology, Validation, Investigation, Writing - review & editing.

Lionel Imbert: Investigation, Writing - review & editing. **Jean-Marie Teulon:** Investigation, Writing - review & editing. **Adrien Favier:** Investigation, Validation, Writing - review & editing. **Jean-Luc Pellequer:** Methodology, Investigation, Validation, Writing - review & editing. **Philippe Huber:** Methodology, Supervision, Validation, Writing - review & editing. **Ina Attrée:** Conceptualization, Supervision, Validation, Project administration, Funding acquisition, Writing - review & editing. **Andréa Dessen:** Conceptualization, Supervision, Validation, Project administration, Funding acquisition, Writing - original draft, Writing - review & editing.

Acknowledgments

We acknowledge the platforms of the Grenoble Instruct-ERIC center (ISBG; UMS 3518 CNRS-CEA-UGA-EMBL) within the Grenoble Partnership for Structural Biology (PSB). Platform access was supported by FRISBI (ANR-10-INBS-05-02) and GRAL, a project of the University Grenoble Alpes graduate school (Ecoles Universitaires de Recherche) CBH-EUR-GS (ANR-17-EURE-0003). The IBS acknowledges integration into the Interdisciplinary Research Institute of Grenoble (IRIG, CEA), and with financial support from the TGIR-RMN-THC Fr3050 CNRS. This work was supported by grant ANR-15-CE11-0018-01 from the Agence Nationale de la Recherche (ANR), including a PhD fellowship to Q.B. Work in the Dessen lab on secretion systems and virulence factors is also supported by grant 2017/12436-9 (ANTIBIO-BAC) from FAPESP (São Paulo Research Foundation). We would like to thank Stéphanie Bouillot for help with lipid raft experiments and preparation of epithelial cells, and the BIOSAXS Beamline team at the ESRF for help with SAXS data collection. This work also acknowledges the AFM platform at the IBS and the Fondation pour la Recherche Médicale (Team FRM 2017, DEQ20170336705). *P. aeruginosa* strain IHMA879472 was kindly provided by the International Health Management Association (IHMA; USA).

CRedit author statement, Bertrand et al

Received 29 February 2020;

Received in revised form 25 May 2020;

Accepted 29 May 2020

Available online 3 June 2020

Keywords:

bacterial infection;
toxin;
type V secretion system (T5SS);
two-partner secretion;
membrane disruption

Abbreviations used:

T3SS, Type III Secretion System; ExlA, Exolysin A; TPS, two-partner secretion; T5SS, Type V Secretion System; CDI, contact-dependent growth inhibition; AFM, atomic force microscopy; SAXS, small-angle X-ray scattering; PA, phosphatidic acid; PI_{xP}, phosphatidylinositols; PS, phosphatidylserine; PC, phosphatidylcholine; DSM, detergent-soluble membrane; DRM, detergent-resistant membrane; M β CD, methyl- β -cyclodextrin; PI, propidium iodide.

References

- [1] Deng, W., Marshall, N.C., Rowland, J.L., McCoy, J.M., Worrall, L.J., Santos, A.S., et al., (2017). Assembly, structure, function and regulation of type III secretion systems. *Nat. Rev. Microbiol.*, **15**, 323–337.
- [2] Pinaud, L., Sansonetti, P.J., Phalipon, A., (2018). Host cell targeting by enteropathogenic bacteria T3SS effectors. *Trends Microbiol.*, **26**, 266–283.
- [3] Elsen, S., Huber, P., Bouillot, S., Coute, Y., Fournier, P., Dubois, Y., et al., (2014). A type III secretion negative clinical strain of *Pseudomonas aeruginosa* employs a two-partner secreted exolysin to induce hemorrhagic pneumonia. *Cell Host Microbe*, **15**, 164–176.
- [4] Reboud, E., Elsen, S., Bouillot, S., Golovkine, G., Basso, P., Jeannot, K., et al., (2016). Phenotype and toxicity of the recently discovered *exlA*-positive *Pseudomonas aeruginosa* strains collected worldwide. *Environ. Microbiol.*, **18**, 3425–3439.
- [5] Basso, P., Ragno, M., Elsen, S., Reboud, E., Golovkine, G., Bouillot, S., et al., (2017). *Pseudomonas aeruginosa* pore-forming exolysin and type IV pili cooperate to induce host cell lysis. *MBio*, **8**, e02250 16.
- [6] Reboud, E., Bouillot, S., Patot, S., Beganton, B., Attree, I., Huber, P., (2017). *Pseudomonas aeruginosa* ExlA and *Serratia marcescens* ShlA trigger cadherin cleavage by promoting calcium influx and ADAM10 activation. *PLoS Pathog.*, **13**, e1006579.
- [7] Basso, P., Wallet, P., Elsen, S., Soleilhac, E., Henry, T., Faudry, E., et al., (2017). Multiple *Pseudomonas* species secrete exolysin-like toxins and provoke caspase-1-dependent macrophage death. *Environ. Microbiol.*, **19**, 4045–4064.
- [8] Delattre, A.S., Saint, N., Clantin, B., Willery, E., Lippens, G., Locht, C., et al., (2011). Substrate recognition by the POTRA domains of TpsB transporter FhaC. *Mol. Microbiol.*, **81**, 99–112.
- [9] Hertle, R., (2002). *Serratia marcescens* hemolysin (ShlA) binds artificial membranes and forms pores in a receptor-independent manner. *J. Membr. Biol.*, **189**, 1–14.
- [10] Meuskens, I., Saragliadis, A., Leo, J.C., Linke, D., (2019). Type V secretion systems: an overview of passenger domain functions. *Front. Microbiol.*, **10**, 1163.
- [11] Guérin, J., Bigot, S., Schneider, R., Buchanan, S.K., Jacob-Dubuisson, F., (2017). Two-partner secretion: combining efficiency and simplicity in the secretion of large proteins for bacteria-host and bacteria-bacteria interactions. *Front. Cell. Infect. Microbiol.*, **7**, 148.
- [12] Grijpstra, J., Arenas, J., Rutten, L., Tommassen, J., (2013). Autotransporter secretion: varying on a theme. *Res. Microbiol.*, **164**, 562–582.
- [13] Leo, J.C., Grin, I., Linke, D., (2012). Type V secretion: mechanism(s) of autotransport through the bacterial outer membrane. *Phil. Trans. R. Soc. Lond. B.*, **367**, 1088–1101.
- [14] da Mata Madeira, P.V., Zouhir, S., Basso, P., Neves, D., Laubier, A., Salacha, R., et al., (2016). Structural basis of lipid targeting and destruction by the type V secretion system of *Pseudomonas aeruginosa*. *J. Mol. Biol.*, **428**, 1790–1803.
- [15] Salacha, R., Kovacic, F., Brochier-Armanet, C., Wilhelm, S., Tommassen, J., Filloux, A., et al., (2010). The *Pseudomonas aeruginosa* patatin-like protein PlpD is the archetype of a novel type V secretion system. *Environ. Microbiol.*, **12**, 1498–1512.
- [16] Ruhe, Z.C., Subramanian, P., Song, K., Nguyen, J.Y., Stevens, T.A., Low, D.A., et al., (2018). Programmed secretion arrest and receptor-triggered toxin export during antibacterial contact-dependent growth inhibition. *Cell*, **175**, 921–933.
- [17] Relman, D.A., Domenighini, M., Tuomanen, E., Rappuoli, R., Falkow, S., (1989). Filamentous haemagglutinin of *Bordetella pertussis*: nucleotide sequence and crucial role in adherence. *Proc. Natl. Acad. Sci. U. S. A.*, **86**, 2637–2641.
- [18] Kajava, A.V., Cheng, N., Cleaver, R., Kessel, M., Simon, M.N., Willery, E., et al., (2001). Beta-helix model for the filamentous haemagglutinin adhesin of *Bordetella pertussis* and related bacterial secretory proteins. *Mol. Microbiol.*, **42**, 279–292.
- [19] Makhov, A.M., Hannah, J.H., Brennan, M.J., Trus, B.L., Kocsis, E., Conway, J.F., et al., (1994). Filamentous hemagglutinin of *Bordetella pertussis*. A bacterial adhesin formed as a 50-nm monomeric rigid rod based on a 19-residue repeat motif rich in beta strands and turns. *J. Mol. Biol.*, **241**, 110–124.
- [20] Clantin, B., H. H. Willery, E., Locht, C., Jacob-Dubuisson, F., Villeret, V., (2004). The crystal structure of filamentous hemagglutinin secretion domain and its implications for the two-partner secretion pathway. *Proc. Natl. Acad. Sci. U. S. A.*, **101**, 6194–6199.
- [21] Konarev, P.V., Volkov, V.V., Sokolova, A.V., Koch, M.H.J., Svergun, D.I., (2003). PRIMUS: a Windows PC-based system for small-angle scattering data analysis. *J. Appl. Crystallogr.*, **36**, 1277–1282.
- [22] Svergun, D.I., (1992). Determination of the regularization parameter in indirect transform methods using perceptual criteria. *J. Appl. Crystallogr.*, **25**, 495–503.
- [23] Mertens, H.D., Svergun, D.I., (2010). Structural characterization of proteins and complexes using small-angle X-ray solution scattering. *J. Struct. Biol.*, **172**, 128–141.
- [24] Ishida, T., Kinoshita, K., (2007). PrDOS: prediction of disordered protein regions from amino acid sequence. *Nucleic Acids Res.*, **35**, W460 W4.
- [25] Schanda, P., Forge, V., Brüttscher, B., (2006). HET-SOFAST NMR for fast detection of structural compactness and heterogeneity along polypeptide chains. *Magn. Reson. Chem.*, **44**, S177–S184.
- [26] De Craene, J.O., Bertazzi, D.L., Bär, S., Friant, S., (2017). Phosphoinositides, major actors in membrane trafficking and lipid signaling pathways. *Int. J. Mol. Sci.*, **15**, E634.
- [27] Vance, J.E., Tasseva, G., (2013). Formation and function of phosphatidylserine and phosphatidylethanolamine in mammalian cells. *Biochim. Biophys. Acta*, **183**, 543–554.
- [28] Lingwood, D., Simons, K., (2010). Lipid rafts as a membrane-organizing principle. *Science*, **327**, 46–50.
- [29] Mahammad, S., Parmryd, I., (2015). Cholesterol depletion using methyl- β -cyclodextrin. *Methods Mol. Biol.*, **1232**, 91–102.
- [30] di Venanzio, G., Stepanenko, T.M., Vescovi, E.G., (2014). *Serratia marcescens* ShlA pore-forming toxin is responsible for

- early induction of autophagy in host cells and is transcriptionally regulated by RcsB. *Infect. Immun.*, **82**, 3542–3554.
- [31] Dal Peraro, M., van der Goot, F.G., (2016). Pore-forming toxins: ancient, but never really out of fashion. *Nat. Rev. Microbiol.*, **14**, 77–92.
- [32] Brothers, K.M., Callaghan, J.D., Stella, N.A., Bachinsky, J. M., AlHigaylan, M., Lehner, K.L., et al., (2019). Blowing epithelial cell bubbles with GumB: ShlA-family pore-forming toxins induce blebbing and rapid cellular death in corneal epithelial cells. *PLoS Pathog.*, **15**, e1007825.
- [33] Hertle, R., (2005). The family of *Serratia* type pore forming toxins. *Curr. Prot. Pept. Sci.*, **6**, 313–325.
- [34] Bryan, A.W.J., Starmer-Kreinbrink, H.L., Hosur, R., Clark, P. L., Berger, B., (2011). Structure-based prediction reveals capping motifs that inhibit β -helix aggregation. *Proc. Natl. Acad. Sci. U. S. A.*, **108**, 11099–11104.
- [35] Bychkova, V.E., Semisotnov, G.V., Balobanov, V.A., Finkelstein, A.V., (2018). The molten globule concept: 45 years later. *Biochemistry (Mosc)*, **83**, S33–S47.
- [36] Baud, C., Guérin, J., Petit, E., Lesne, E., Dupré, E., Locht, C., et al., (2014). Translocation path of a substrate protein through its Omp85 transporter. *Nat. Commun.*, **5**, 5271.
- [37] Nash, Z.M., Cotter, P.A., (2019). *Bordetella filamentous* hemagglutinin, a model for the two partner secretion pathway. *Microbiol. Spectr*, **7**, PSIB-0024-2018.
- [38] Bouillot, S., Reboud, E., Huber, P., (2018). Functional consequences of calcium influx promoted by bacterial pore-forming toxins. *Toxins*, **10**, E387.
- [39] Trouillon, J., Sentausa, E., Ragno, M., Robert-Genthon, M., Lory, S., Attrée, I., et al., (2020). Species-specific recruitment of transcription factors dictates toxin expression. *Nucleic Acids Res*, **28**, 2388–2400 epub.
- [40] Franke, D., Petoukhov, M.V., Konarev, P.V., Panjkovich, A., Tuukkanen, A., Mertens, H.D.T., et al., (2017). ATSAS 2.8: a comprehensive data analysis suite for small-angle scattering from macromolecular solutions. *J. Appl. Crystallogr.*, **50**, 1212–1225.
- [41] Burgess, R.R., (2009). Refolding solubilized inclusion body proteins. *Methods Enzymol.*, **463**, 259–282.
- [42] Berry, A., Han, K., Trouillon, J., Robert-Genthon, M., Ragno, M., Lory, S., et al., (2018). cAMP and Vfr control exolysin expression and cytotoxicity of *Pseudomonas aeruginosa* taxonomic outliers. *J. Bacteriol.*, **200**, e00135 18.
- [43] Nečas, D., Klapetek, P., (2012). Gwyddion: an open-source software for SPM data analysis. *Cent. Eur. J. Phys*, **10**, 181–188.
- [44] Chen, S.W., Pellequer, J.L., (2011). DeStripe: frequency-based algorithm for removing stripe noises from AFM images. *BMC Struct. Biol.*, **11**, 7.
- [45] Chen, S.W., Teulon, J.M., Godon, C., Pellequer, J.L., (2016). Atomic force microscope, molecular imaging, and analysis. *J. Mol. Recognit.*, **29**, 51–55.